Static and dynamic analysis of bending–torsion coupling of a CFRP sandwich beam

Loïc Bernard, Guilhem Michon, Rached El Fatmi, Bruno Castanié

STATIC AND DYNAMIC ANALYSIS OF BENDING-TORSION COUPLING OF A CFRP SANDWICH BEAM

Loïc Bernard†‡, Guilhem Michon†, Rached El Fatmi*, Bruno Castanié†

†Université de Toulouse; ICA (Institut Clément Ader); INSA, ISAE, UPS, Mines Albi;

3 rue Caroline Aigle, 31400 Toulouse, France

*** ENI Tunis, Le Belvédère, BP 37, 1002 Tunis, Tunisie**

Abstract

The bending-torsion coupling for a sandwich beam is analysed from the static and vibrational point of view. Off-axis orientations in the skin and transverse graded core are proposed to perform the coupling. Solutions are first compared numerically from a static point of view using a complete beam theory. The natural frequencies and mode shapes are then studied experimentally and numerically. An experimental assembly test rig is presented, where a sandwich beam is embedded on the shaker and measurements are taken with a scanning vibrometer. These results are then compared to those calculated by a finite element model in order to verify the accuracy of the model and its ability to consider all the physical phenomena involved.

† Corresponding author: bruno.castanie@insa-toulouse.fr

1 Introduction

Laminated composite beams have been used in numerous engineering applications in many fields such as aeronautics, wind energy, and automotive engineering. These structures, composed of composite materials, have lower weight, better fatigue life and higher strength and stiffness than those composed of metallic materials. Moreover, composite structures can be tailored to different needs by using different stacking sequences, local reinforcements, and many coupling deformations, which take advantage of the anisotropy of the materials. These abilities have permitted composite materials to replace metallic materials on a large scale. The rise of composite components in Airbus Aircraft, from the A319 to the A350, is a good illustration of such evolution.

The aim of this paper is to focus on how bending-torsion coupling can be created and what its impact will be on dynamic behaviour in the case of a sandwich beam. In the literature, bending-torsion coupling of beams is mainly considered in the aeronautical and wind energy fields. In the field of helicopters, this coupling has been largely investigated for rotor stability, vibration reduction and flutter issues. Panda and Chopra [1] highlighted the great potential of bending-torsion coupling for rotor stability and vibration level. Chandra and Chopra [2] proposed an analytical model based on Vlasov theory to take static deformation due to elastic couplings into account. Then Chopra and Smith [3] investigated the impact of elastic couplings on blade aeroelastic response and dynamic loads in the case of a soft-in-plane hingeless rotor. In their works, they applied elastic couplings on the upper and lower walls of the torsional box, which is part of the internal blade structure. To optimize bending-torsion coupling of the structural boxes, an optimization function based on vibration level and rotor stability parameters has been developed to obtain the best box walls stacking sequence combination, composed of un-balanced plies set at 15°. Ganguli and Chopra [4,5] developed and tested a new internal structure for the blade, which was composed of two horizontal

torsional boxes. They managed to reduce the vibration levels and dynamic loads at the rotor hub even further. They then added design variables to the optimization function [6], including ply angles of the laminated walls of the box beam, sweep, anhedral and planform taper, and non-structural mass. Murugan and Ganguli [7] updated the optimization procedure to decrease the vibration level of a four-bladed soft-in-plane rotor, by 15%, by using bending-torsion effects. Guo et al. [8] studied the effect of bending-torsion coupling on the flutter speed. They managed to show a significant improvement of the wing flutter speed in presence of coupling in the central wing torsion box. They used an asymmetric lay-up for all torsional box walls, composed of plies at 30° and -30° for the front and rear spars.

In the renewable energy field, wind turbine blades also need to be tailored to different situations. The main issues are to maintain constant energy production under wind gusts or a wind speed gradient between the ground and the top of the turbine. Bending-torsion coupling is used to passively twist the blade so that it adapts to wind variations. The first work on tailoring wind turbine blades was performed by Koraolis et al. [9], who tested various orientations of blade skin layers to tailor the rotor in order to overcome wind turbine overloading. Kooijman [10] based his work on [9] to study the effect of bending–torsion coupling on wind turbine efficiency. He succeeded in increasing the wind turbine efficiency by 10% without any change to the blade's angle of attack or the rotor speed. De Goeij et al [11] showed the interest of bending-torsion coupling for the blade fatigue life. They compared three different torsional box architectures and showed that a vertically coupled torsional box was more efficient to introduce coupling. Griffin [12] proposed a new architecture for blade structure by introducing a mix of off-axis orientated skin plies composed of glass fabric and carbon fabric, and a coupled torsional box. The skin was composed of carbon fabrics orientated at 20°and glass fabrics at -70°. Nicholls-Lee et al. [13] studied the application of bending-torsion coupling to tidal turbines. Their objectives were to increase the turbine

fatigue life and the power captured. They used a torsional box tailored by setting the outer plies at 90°, the middle plies at 20° and the inner plies at 45°. An increase of 2.5% was achieved for the energy captured and a decrease of thrust loading of about 10% was obtained.

Most of this literature reports work done on bending-torsion coupling, in engineering fields, focused on the torsional box. In aeronautics, sandwich structures are widely used, in panels for example, and constitute an interesting alternative line of investigation.

All couplings can be identified in extra-diagonal terms of the beam stiffness matrix (Figure 1). The couplings are largely influenced by the sectional geometry as well as in- and out-of-plane warping, Poisson's effect and transverse shear. For this reason, an accurate composite beam theory able to calculate the stiffness matrix and beam deformation for an arbitrary beam cross section is required for this investigation of sandwich elastic coupling.

Figure 1 here

In this paper only bending-torsion coupling will be treated. Two types of this kind of coupling can be extracted from the stiffness matrix. The first one, called structural coupling, is illustrated by the K_{45} term and the second one, called inertial coupling, can be symbolized by the K_{34} term. These two parameters have great significance for the design of rotor blades.

Structural bending-torsion coupling can be presented as in Figure 2. The centre of gravity (CG) and centre of torsion (CT) are at the same point. If bending momentum is applied to the structure, rotation of the section is induced.

Figure 2 here

Inertial coupling is illustrated in Figure 3. In this case, the centre of gravity (CG) and centre of torsion (CT) are not at the same position. If a shear force is applied to the structure, an induced torsion rotation of the section is created.

Figure 3 here

Finding way of calculating 2D cross-sectional properties which is able to take coupling effects, and in-plane and out-of-plane warping, into account is an important problem in composite structural design. An efficient composite beam theory must also be able to express the 3D deformation behaviour by including transverse shear effects, constrained warping, cross sectional distortion, Poisson's effects and the influences of all boundary conditions. A large number of composite beam theories have been developed in recent decades. Only three of them will be briefly presented here.

The first theory comes within the framework of high order composite beam theory and was developed in the late 1990's by Barrau et al. [14, 15]. This theory does not consider any homogenization of the composite material's properties and an out-of-plane warping function is introduced in the displacement field. The displacement is split into a rigid and a variable part. The rigid part allows the determination of six coefficients, which can be found through 2D finite element method analysis. Once these coefficients have been calculated, the global problem can be solved. This method gives good results but the warping effects are approximated and the Poisson's coefficient effects are not taken into account. This theory can only be applied to straight beams of arbitrary cross section, with no twist.

The second theory is "Variational asymptotic beam theory" developed by Hodges and his co-workers [16]. It is based on a variational asymptotic method [17] which consists of splitting the 3D problem into a 2D linear and a 1D non-linear problem. In this theory, assumptions are also made on the displacement field, which is based on the generalized Timoshenko form. The 2D cross section analysis is made via a finite element calculation. The 1D non-linear problem is an approximation of the 3D body strain energy. This gave birth to software named VABS, which is able to calculate twisted, curved beams with arbitrary cross sections. It has been updated many times to improve the accuracy [18].

The third theory is “Exact composite beam theory” developed by Ladevèze and Simmonds [19] and extended by El Fatmi [20-22]. This theory is based on the 3D Saint Venant’s problem. Far from the boundary conditions, the local equilibrium equation is the exact solution of the 1D Saint-Venant’s problem. The beam 3D strain and stress is obtained using the 1D displacement without any hypothesis. To solve the 1D problem, a pair of linear operators need to be calculated. El Fatmi found a way to obtain these linear operators using finite elements and computed the entire theory in his own software called *Csection/Cbeam* [23]. This software is able to take account of in- and out-of-plane warping, Poisson’s effects and disruptions produced by boundary conditions. Moreover, this theory is suitable for any arbitrary cross section of straight beams. Thus, *Csection* seems to be the most appropriate software for studying interactions between structural and inertial bending-torsion couplings. It can be applied to various cross sectional geometries without making any displacement hypothesis for static stresses.

According to the literature, in the case of a box beam, off-axis plies are an efficient solution, which will also be tested in our case. A more original technique is the use of a horizontally graded core to enhance the coupling coefficients. The authors have not found any reference to this possibility except in the aim of smoothing the stress around inserts in sandwich structures [24]. In fact, most authors have focused on a vertically graded core [25-28] and most often from a static point of view. In the next subsection, the bending-coupling of some sections will analysed from a static point of view to find the best design. The third part of the paper will explore the association of structural and inertial bending-torsion coupling in dynamic response for a range of selected sandwich beams. An original campaign of dynamic experiments without intrusive experimental measurements is proposed to validate the numerical results. Finally some conclusions will be drawn.

2 Static investigation

A numerical static investigation was first performed to assess the capability and the relative performance of the designs proposed. Three configurations with horizontally graded cores (box, elliptical and sandwich) are illustrated in Figure 4. The stacking was composed of a balanced 45° fabric ply (TC 45°) made of carbon with an epoxy resin and an off-axis ply (TC θ°) made of the same material. Two different densities of foams were used: 65 and 200 kg/m^3

Figure 4 here

The beam dimensions used for this static campaign were the following:

- Beam length: 600 mm
- Beam width: 80 mm
- Carbon ply thickness: 0.35 mm
- Foam core thickness: 20 mm
- Total beam thickness: 21.4mm

The literature shows that most coupling angles for carbon plies are set between 15° and 30°. In this work, the off axis angle was set at 20°. The association of low density foam with high density foam was chosen to characterize the vertically graded core.

In this static numerical campaign, all beams were in a clamp-free configuration. A single upward force was applied along the geometric centre axis on the upper surface, at the beam tip (Figure 5).

Figure 5 here

Stiffness matrixes were calculated using [23] to investigate the effects of both off-axis ply and vertically graded core on the cross section geometries. Inertia and structural bending-torsion

coupling were expressed according to the torsional stiffness of the section in order to highlight coupling in proportion (Table 1).

Table 1 here

In Table 1, the box section structure can be seen to have the lowest measured beam twist rate because of its natural torsional stiffness. Moreover the inertia bending-torsion term is almost zero. In the elliptical configuration the torsional stiffness is slightly lower than in the box configuration. The comments that can be made for this cross section are similar to those for the box configuration. The sandwich section is less rigid in torsion because it is, in fact, an open section and is the only configuration that allows the graded core to express itself. The K_{43} term is relatively small compared to the K_{45} term but at least it is not close to zero. The K_{45} term also has a higher value than the other two configurations.

The respective contributions of the off axis ply and the horizontally graded core to the beam twist rate are given in Table 2.

Table 2 here

This shows that closed box structures generate quite a low beam twist rate, whereas the sandwich structure generates a much higher one. The high torsional stiffness and the weak value of the K_{34} term induced by box and elliptical configurations (Table 1) feed through to the influence on the beam twist rate. Thus, the horizontally graded core has no influence on the total beam twist rate. In the case of the sandwich structure, the total twist rate is twice that of the other configurations. Moreover, the influence of the graded core is significant in creating such coupling.

This study shows that the sandwich configuration seems to be the best for studying interactions between inertia and structural bending-torsion coupling. So, four configurations were selected (Figure 6). The first configuration, called the “reference” beam, was a simple sandwich beam with 0/90° angle for the outer ply and ±45° for the inner ply of both skins. In

this configuration, the sandwich core was composed only of low density foam. All the other configurations were compared to this reference beam. In the second configuration, the outer ply of both skins was made of woven carbon fabric orientated at +20°/-70°. The third configuration was composed of two foams with different mechanical properties within the width of the sandwich core. Finally, the fourth configuration was a combination of both technical solutions. This skin/core arrangement was identified as the most coupled configuration with the highest induced twist rate in the static campaign.

Figure 6 here

3 Dynamic experiments and modelling

3.1 Specimen manufacturing

The specimens were manufactured using the following procedure:

- Foam blocks were first precisely machined.
- Two sacrificial foam blocks coated with release films were added, one on either side. The objective was to have more precise control over the shape and the dimensions of the skins after curing and trimming.
- Upper and lower carbon plies were set on the top and bottom of the beam.
- An aluminium pad was added at the beam root to clamp the beam without destroying the structure.
- The aluminium pad and foam blocks were stuck together (Figure 7) using a Redux film.

Figure 7 here

Then the assembly was prepared for curing:

- All sandwich beam elements were placed between two rigid metallic plates surrounded by a plastic film so that a vacuum could be applied.
- The role of the vacuum was to keep all the elements together during curing in order to use the extra resin of the pre-peg to stick the carbon plies and foam blocks together.
- The conditioned beam assembly was then placed in the oven and a specific curing cycle was applied.

Once the sandwich beam had been cured, the foam blocks were removed from both sides and the extra width of carbon plies was cut off to obtain the final result (Figure 8).

Figure 8 here

3.2 Experimental setting

In order to test the bending-torsion coupling in vibration, the sandwich beam had to be excited only in pure bending to obtain the induced torsion response. Therefore the sandwich beam was embedded on a horizontal plate directly connected to an electrodynamic shaker (Figure 9). In that way, the excitation along the z axis was directly applied to the clamp and no parasite excitation occurred. The input signal was considered as a pure bending excitation. Compared to a modal test, this setup did not introduce the local mass and stiffness due to fixation of the shaker on the studied zone that usually changes the dynamic response of the beam.

Figure 9 here

The system was controlled by an accelerometer set directly on the clamp. Another accelerometer was installed to measure the beam response and thus find the beam Frequency Response Function (FRF). An initial sine sweep from 0 Hz to 1000 Hz was performed to extract the natural frequency according to the response at a single output point. To obtain the mode shapes, a second test used pure sinusoidal excitation on each previously identified

natural frequency. The modal deformation was obtained by means of a laser vibrometer that scanned 36 points of a predefined mesh. Here, only the first six mode shapes will be treated.

3.3 Numerical modelling

A finite element model was developed to be able to study the coupling with other beam configurations numerically. The 3D model, developped with Samcef Software [29], used solid elements to mesh the sandwich core and composite solid elements for both carbon skins. The integration rule for the thickness was applied layer by layer to obtain a better transverse shear stress and normal stress gradient in the skins. A convergence study (by comparison with the results of Subsection 2) was performed and led to 8 elements in the thickness of the core and one element for each skin. 20 elements were used in the width, leading to a model with 200 000 degrees of freedom, see Figure 10.

Figure 10 here

The dynamic behaviour of the sandwich was computed using the Samcef *Dynam* and *Repdyn* modules:

- The *Dynam* module allows the dynamics of a model to be characterized by determining the natural frequencies and effective masses for each eigenfrequency. The effective masses allow the mode shape to be identified by expressing mass fractions in translation and rotation movement.
- The *Repdyn* module performs harmonic excitation to obtain the Frequency Response Function (FRF). The resolution method is based on the Lanczos method, in which resolution is extremely quick and does not imply high CPU cost. This method is well suited for mode shape calculations of models with high numbers of DOF. The computational time is about 10 min on 4 cores.

The assumption was made that none of the material was frequency-sensitive. This assumption was verified for the two foams with Dynamic Material Analysis (DMA) tests that are not reported here. This finite element methodology will be validated in the next section.

4 Results and discussions

4.1 Frequency Response Function

The FRFs were obtained following the experimental protocol described previously. The excitation was performed directly at the clamp in the *y* direction only, in order to simulate an excitation in bending. The FRF was measured at the top left corner of the clamped beam by the vibrometer. The same position was chosen on the numerical model.

Figure 11 here

In the set of FRF graphs (**Figure 11**), simulation and experimental curves were superposed and showed good agreement between experiment and the 3D model. In most cases, peak amplitudes were slightly overestimated in the model. Natural frequencies were correctly positioned and will be detailed numerically in the next section. Note that the presence of the graded foam core significantly changed the FRF curve profile (*Types 3* and *4*). An extra peak appeared at around 250 Hz and around 800 Hz.

Natural frequencies were compared in terms of number and to quantify the gap between experimental and simulation results. Table 3 shows simulated eigenfrequencies for all the types of configurations related to experiment. As described above, the gap between experimental and simulated eigenfrequencies was very small. It is interesting to note that the first results obtained displayed a larger gap for *Type 3* and *4* sandwich beams. After further investigations, it appeared that the high density foam had not been adequately characterized

and induced larger differences, of about 15%. After re-testing by DMA, a new value of the stiffness coefficient for high density foam was found and the gap dropped to less than 3%. It can thus be concluded that the foam core plays a very important role in sandwich beam dynamics.

Table 3 here.

From Table 3 and the FRF curves of **Figure 11**, it can be seen that the ply oriented at 20° did not influence the positions of the frequency modes except for the first mode, as attested by the eigenfrequencies of type 1 and type 2 beams. Modes 3 and 6 are not represented on the FRF curves meaning that those modes are superposed by mode 2 and 5**.** In the presence of a graded core, the FRF profiles changed significantly. The FRF curve of type 3 beam shows 3rd and 6th mode peaks. The added mass and the higher stiffness introduced by the high density foam increased all eigenfrequencies modes and increased the gap between modes 2 and 3 and between 5 and 6.

4.2 Mode shape analysis

Experimental and numerical mode shapes were compiled on the same graph so that they could be compared visually as illustrated in Figure 12 and Figure 13. In this section, only the modal deformations of the *Type 1* (uncoupled) (Figure 12) and *Type 4* configurations (fully coupled) (Figure 13) are displayed. Strong similarities of the modal deformations of *Type 2* and *3* configurations with those of the Type 4 configuration allow us to display only those given by the fully coupled arrangement.

Figure 12 here

Note that torsional deformations are not shown in Figure 12. The lack of coupling between bending and torsion and the pure excitation in bending led to very weak excitation of torsional modes.

Figure 13 here

Concerning the fully coupled configuration, good mode shape correlation between experiment and simulation was reached for the first 6 modes (Figure 13). Introduction of coupling solutions in a sandwich beam structure proved that bending-torsion coupling could be generated. The difficulty lay in the quantification of the amount of bending and torsion deformation within the eigenmode.

Usually the Modal Assurance Criterion (MAC) is used to correlate modal deformation between simulation and experiment. The use of this criterion is based on eigenvectors as in the following equation [30,31].

$$MAC\left(\Phi_{i\underline{k}}, \Phi_{i\underline{l}}\right) = \frac{\left(\Phi_{\underline{k}i}, \Phi_{i\underline{l}}\right)^2}{\left(\Phi_{\underline{k}i}, \Phi_{i\underline{k}}\right)\left(\Phi_{\underline{l}i}, \Phi_{i\underline{l}}\right)}$$

$\Phi_{i\underline{k}}: Eigenvectors\ from\ the\ simulation\ software$
$\Phi_{i\underline{l}}: Eigenvectors\ from\ the\ experiment$

The MAC matrix gives a good overall view of the shape correlation and this is the basis of the derived MAC method, called the identification matrix, to quantify coupling deformation within an Eigen mode. The technique uses a non-coupled sandwich beam as the reference with which each coupled beam is compared. The matrix is also expressed in percentages for a better representation.

Input parameters to the identification matrix come from:

$\Phi_{i\underline{k}}: Eigenvectors\ from\ the\ experimental\ Reference\ configuration\ (type\ 1)$
$\Phi_{i\underline{l}}: Eigenvectors from\ the\ experimental\ Coupled\ configuration\ (type\ 4)$

In Table 4, the reference deformation shape is symbolized by one letter and one number. The letter *T* stands for Torsion deformation and *B* for Bending deformation. The number that follows determines the mode numbers. For example *B2* means the second mode of bending.

Using the visualization of coupled mode from the previous paragraph, the MAC matrix for each configuration is presented below. These matrices and their comparisons will contribute to an understanding of the influence of the orientated ply and the graded foam core on the amount of bending and torsion within the first 6 modes.

Tables 4, 5, 6 here.

With this method, it is easy to determine the amount of bending and torsion in each mode. For example, the second mode of the *Type 2* beam (Table *4*) is composed of 55% of torsional deformation and 45% of bending deformation. In the case of a type 3 beam (Table *5*) mode 2 is composed of 65% of torsional deformation and 35% of bending deformation. Another specificity of a type 2 beam is the creation of bending-torsion coupling for modes 5 and 6. This coupling is not present for the beam without orientated ply as shown by the MAC matrix for type 3 beams. This coupling is also present in type 4 sandwich beams (Table *6*) with the same proportions, which means that it is a pure effect of off-axis plies and is not affected by the vertically graded core. However, for this configuration, an uncoupling phenomenon occurs for modes 2 and 3. For example mode 2 is now mainly composed of bending deformation (85% of B2 and 15% of T1) and mode 3 of torsional deformation (85% of T1 and 15% of B2). Such behaviour is called mode veering. This phenomenon occurs when two eigenmodes are very close in frequency as described in Gallina's work [32].

According to the identification matrix, mode 2 of the type 4 beam looks very similar to mode 3 of the sandwich beam composed of either the orientated ply or gradient foam core.

To recover strong coupling for the beam with both technologies, another configuration was tested. The orientated ply was reoriented to -20°/70, which meant that the ply angle of rotation was anticlockwise and both foams kept the same position as shown in Figure 14.

Figures 14 and 15 here

The FRFs curves of Figure 15 illustrate the changes the new skin plies orientation (Type 5) and the inversion of the graded foam core (Type 6). The new ply orientation involves almost no changes on the FRF profile whereas the inverse graded foam core (GFC) significantly modifies the amplitude of coupled modes 2, 3 and 6. In type 4 and 5 FRF curves, mode 3 has smaller amplitude than mode 2 whereas, in type 6, the amplitude of mode 3 is clearly higher. The same phenomenon can be observed for the coupling between modes 5 and 6.

The identification matrix thus becomes (Table 7).

Table 7 here.

The changes made in type 5 and type 6 configurations significantly modified the bending-torsion coupling for modes 2 and 3. The distribution was then 40% torsion deformation and 60% bending deformation for mode 2. However, mode veering was still present. The second degree of bending-torsion coupling between modes 5 and 6 kept the same proportion as in the type 2 beam configuration and remained unchanged whatever the configuration.

5 Conclusion

The aim of the paper was to present a way to generate bending-torsion coupling for a sandwich beam structure. This coupling was introduced into the sandwich structure by means of an outer, orientated carbon fabric ply in both skins and a horizontally graded foam core having 2 different foam characteristics. An experimental protocol for measuring beam deformations, FRF and mode shapes accurately were also presented. This original setup, in which the beam was excited directly at its clamp, allowed the induced torsion of the coupled structure to be expressed. Good correlation was obtained between the 3D numerical model and experimental results. Different configurations were tested to better understand the influence of each nature of bending-torsion coupling and their associations. This experimental process highlighted a mode veering phenomenon when both technologies were introduced in the structure. The identification matrix method allowed to quantify bending-torsion coupling for each configuration and highlighted the fact that fully coupled static configurations may not be suitable for optimum dynamic coupling. Another configuration was found to restore strong modal coupling within the sandwich structure with both technologies.

6 Bibliography

[1] Panda B, Chopra I. Dynamics of Composite Rotor Blades in Forward Flight. Vertica 1987; 11(1/2):187‐210.

[2] Chandra R, Chopra I. Structural Response of Composite Beams and Blades with Elastic Couplings. Compos. Eng. 1992; 2(5/7):347‐374.

[3] Chopra I, Smith EC. Aeroelastic Response, Loads, and Stability of a composite Rotor in Forward Flight. AIAA Journal 1993;31:1265‐1273.

[4] Ganguli R, Chopra I. Aeroelastic Optimization of a Helicopter Rotor with Two-Cell Composite Blades. AIAA Journal 1996;34(4):835‐841.

[5] Ganguli R, Chopra I. Aeroelastic Optimization of a Helicopter Rotor to Reduce Vibration and Dynamic Stresses. Journal of Aircraft 1996;33(4):808‐815.

[6] Ganguli R, Chopra I. Aeroelastic Tailoring of Composite Couplings and Blade Geometry of a Helicopter Rotor Using Optimization Methods. Journal of American Helicopter Society 1997;42(3):218‐228.

[7] Murugan S, Ganguli R. Aeroelastic Stability Enhancement and Vibration Suppression in a Composite Helicopter Rotor. Journal of Aircraft 2005;42(4):1013‐1024.

[8] Guo SJ, Bannerjee JR, Cheung CW. The Effect of Laminate Lay-Up on the Flutter Speed of Composite Wings. Journal of Aerospace Engineering 2003;217(3):115‐122.

[9] Koraolis NM, Mussgrove PJ, Jeronimidis G. Active and Passive Aeroelastic Power Control using Asymmetric Fibre Reinforced Laminates for Wind Turbine Blades. 10th British Wind Energy Conference. London, 1988.

[10] Kooijman HJT. Bending-Torsion Coupling of a Wind Turbine Rotor Blade. Smart Rotor Project, 1996.

[11] De Goeij WC, Van Tooren MJL, Beukers A. Implementation of Bending-Torsion Coupling in the Design of a Wind-Turbine Rotor-Blade. Applied Energy 1999;63(3):191‐207.

[12] Griffin DA. Evaluation of Design Concepts for Adaptive Wind Turbine Blades. Sandia National Laboratories 2002. p. 19.

[13] Nicholls-Lee RF, Turnock SR, Boyd SW. Application of Bend-Twist Coupled Blades for Horizontal Axis Tidal Turbines. Renewable Energy 2013;50:541‐550.

[14] Sudre M, Barrau JJ. Determination du Tenseur Complet des Contraintes dans des Poutres Composites. 10ième Journées nationales sur les composites 1996;10:847‐856.

[15] Taufik A, Barrau JJ, Lorin F. Composite Beam Analysis with Arbitrary Cross Section. Composite Structures 1999;44(2/3):189‐194.

[16] Cesnik CES, Hodges DH. VABS: A New Concept for Composite Rotor Blade Cross-Sectional Modeling. Journal of American Helicopter Society 1997;42(1):27‑38.

[17] Berdichevsky VL. Variational-Asymptotic Method of shell Theory Construction. PMM 1979;43(4):664‑687.

[18] Yu W, Hodges DH, Ho JC. Variational Asymptotic Beam Sectional Analysis – An Updated Version. International Journal of Engineering Science 2012;59:40‑64.

[19] Ladevèze P, Simmonds J. New Concepts for Linear Beam Theory with Arbitrary Geometry and Loading. European Journal of Mechanics - A-Solids 1998;17(3):377‑402.

[20] El Fatmi R, Zenzri H. A Numerical Method for the Exact Elastic Beam Theory. Applications to Homogeneous and Composite Beams. International Journal of Solids and Structures 2004;41(9/10):2521‑2537.

[21] El Fatmi R, Ghazouani N. Higher order composite beam theory built on Saint-Venant's solution. Part-I: Theoretical developments. Composite Structures 2011;93(2):557-566.

[22] Ghazouani N, El Fatmi R. Higher order composite beam theory built on Saint-Venant's solution. Part-II: Built-in effects influence on the behavior of end-loaded cantilever beams. Composite Structures 2011;93(2):567-581.

[23] El Fatmi R. A new tool for composite beam computation. JEC Composite Magazine 2013;85:54.

[24] El Fatmi, R. A Matlab Tool to Compute the Mechanical Characteristics of Any Composite Section. Journal of Composite and Advanced Materials, RCMA 2012;22(3):395-413.

[25] Bozhevolnaya E, Lyckegaard A. Structurally graded core inserts in sandwich panels. Composite Structures 2005;68(1):23-29.

[26] Venkataraman S, Sankar BV. Elasticity Solution for Stresses in a Sandwich Beam with Functionally Graded Core. AIAA Journal 2003;41(12):2501‑2505.

[27] Zhu H, Sankar BV. A Combined Fourier Series–Galerkin Method for the Analysis of Functionally Graded Beams. Journal of Applied Mechanics 2004;71(3):421‑424.

[28] Rahmani O, Khalili SMR, Malekzadeh K, Hadavinia H. Free Vibration Analysis of Sandwich Structures with a Flexible Functionally Graded Syntactic Core. Composite Structures 2009;91(2):229‑235.

[29] SAMCEF User Manuel 14.1.

[30] Allemang RJ. The Modal Assurance Criterion (MAC): Twenty Years of Use and Abuse. Sound and Vibrations 2003;20:14-21.

[31] Girard A, Roy N. Dynamique des Structures Industrielles. Paris : Hermes Science Publications 2003.

[32] Gallina A, Pichler L, Uhl T. Enhanced Meta-Modelling Technique for Analysis of Mode Crossing, Mode Veering and Mode Coalescence in Structural Dynamics. Mechanical Systems and Signal Processing 2011;25(7):2297-2312.

FIGURES

$$\begin{matrix} \textit{Shear forces} \\ \\ \\ \textit{Moments} \\ \\ \\ \end{matrix} \left\{ \begin{bmatrix} N_x \\ T_y \\ T_z \\ M_t \\ M_y \\ M_z \end{bmatrix} = \begin{bmatrix} K_{11} & K_{12} & K_{13} & K_{14} & K_{15} & K_{16} \\ K_{21} & K_{22} & K_{23} & K_{24} & K_{25} & K_{26} \\ K_{31} & K_{32} & K_{33} & K_{34} & K_{35} & K_{36} \\ K_{41} & K_{42} & K_{43} & K_{44} & K_{45} & K_{46} \\ K_{51} & K_{52} & K_{53} & K_{54} & K_{55} & K_{56} \\ K_{61} & K_{62} & K_{63} & K_{64} & K_{65} & K_{66} \end{bmatrix} \cdot \begin{bmatrix} \Delta_x \\ \gamma_y \\ \gamma_z \\ \chi_x \\ \chi_y \\ \chi_z \end{bmatrix} \right\} \begin{matrix} \\ \\ \\ \textit{Translations} \\ \\ \\ \textit{Rotations} \end{matrix}$$

$\mathbf{K_{12}}$: *Extension - Lag coupling*
$\mathbf{K_{13}}$: *Extension - Flap coupling*
$\mathbf{K_{14}}$: *Extension - Torsion coupling*
$\mathbf{K_{25}}$: *Lag shear - Flap bending coupling*
$\mathbf{K_{34}}$: *Flap shear - Torsion coupling*
$\mathbf{K_{36}}$: *Flap shear - Lag bending coupling*
$\mathbf{K_{45}}$: *Flap bending - Torsion coupling*
$\mathbf{K_{46}}$: *Lag bending -Torsion coupling*

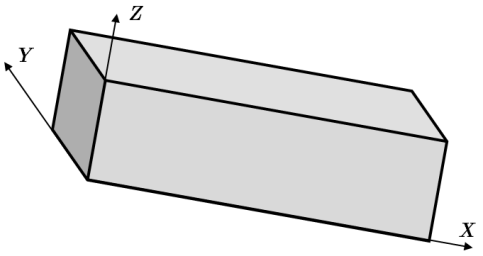

Figure 1 : Representation of the stiffness matrix

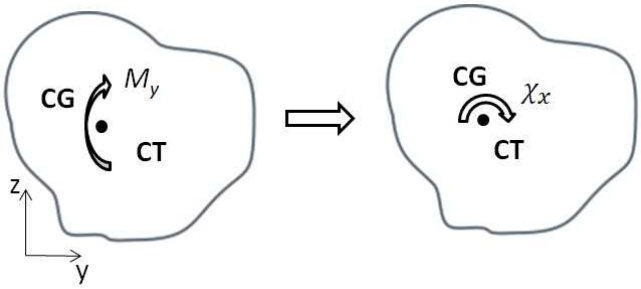

Figure 2 : Structural bending-torsion coupling (K45)

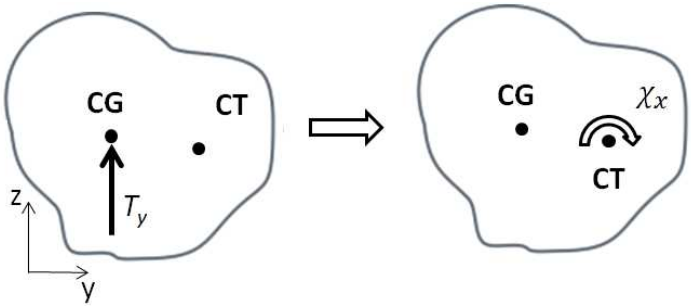

Figure 3 : Inertial bending-torsion coupling (K43)

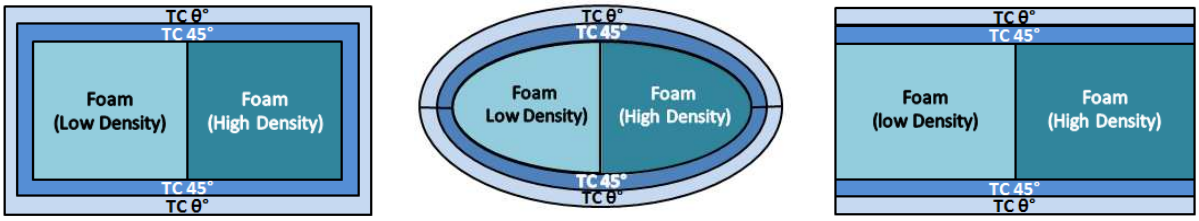

Box configuration *Elliptical configuration* *Sandwich configuration*

Figure 4 : Illustration of the three configurations

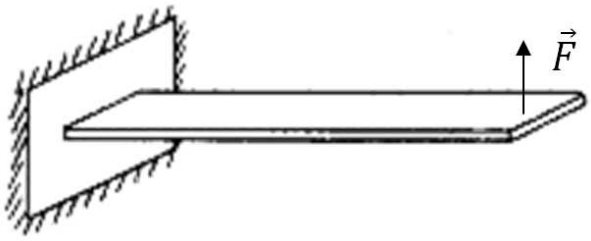

Figure 5 : Illustration of the static boundary conditions

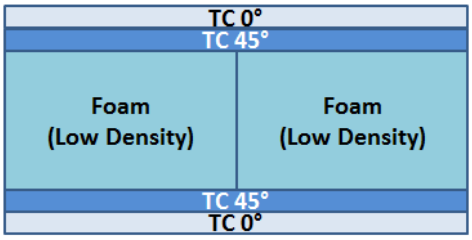

Type 1 (Reference beam)
Skin : External carbon ply at 0°/90°
Core : Homogeneous low density foam core

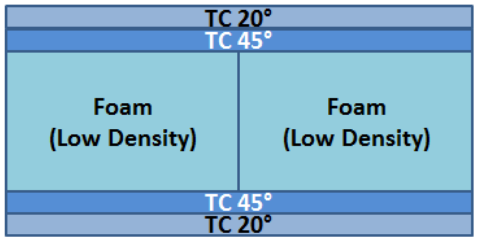

Type 2 (Orientated ply)
Skin : External carbon ply at +20°/-70°
Core : Homogeneous low density foam core

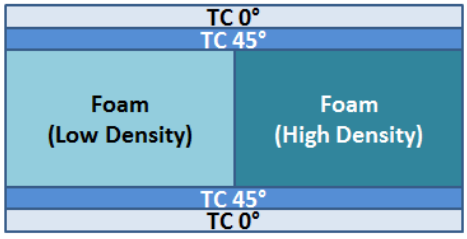

Type 3 (Foam density gradient)
Skin : External carbon ply at 0°/90°
Core : Graded foam core

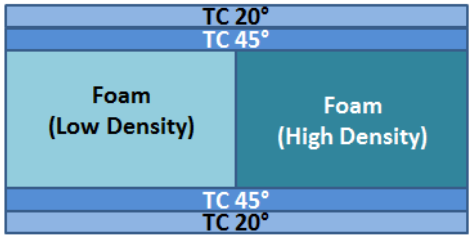

Type 4 (Fully coupled beam)
Skin : External carbon ply at +20°/-70°
Core : Graded foam core

Figure 6 : Sandwich beam configurations studied

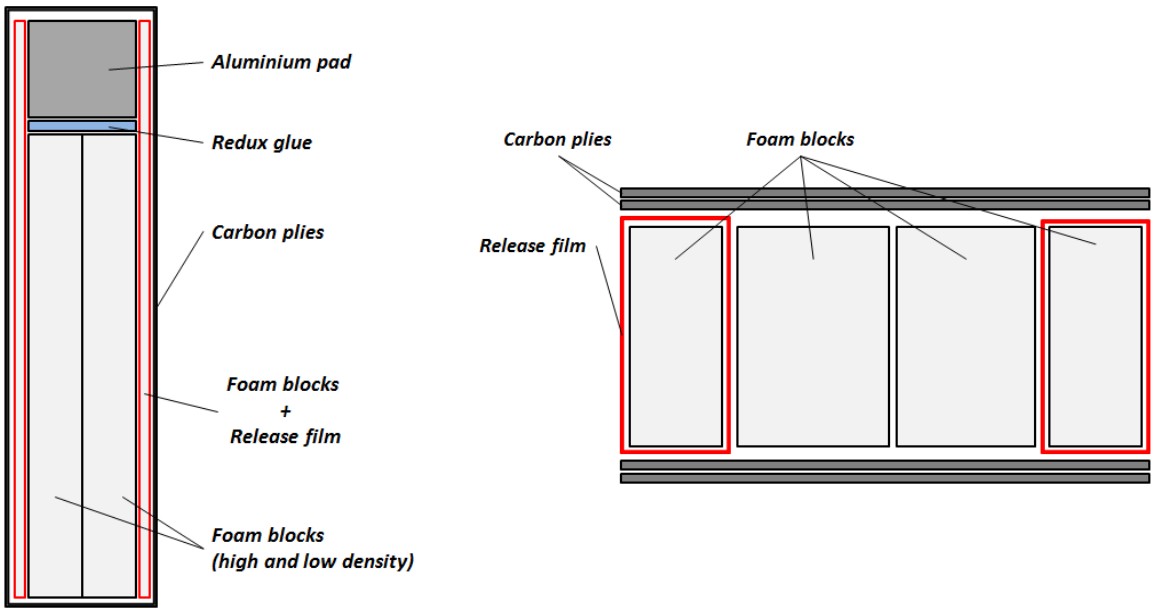

a) Upper view of the assembly *b) Front view of the assembly*

Figure 7 : Sandwich beam elements assembly

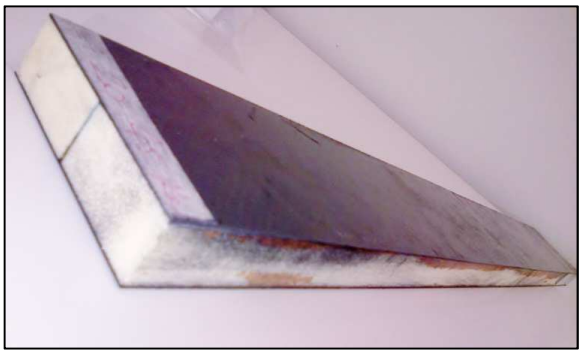

Figure 8: Fully coupled sandwich beam ready to be tested

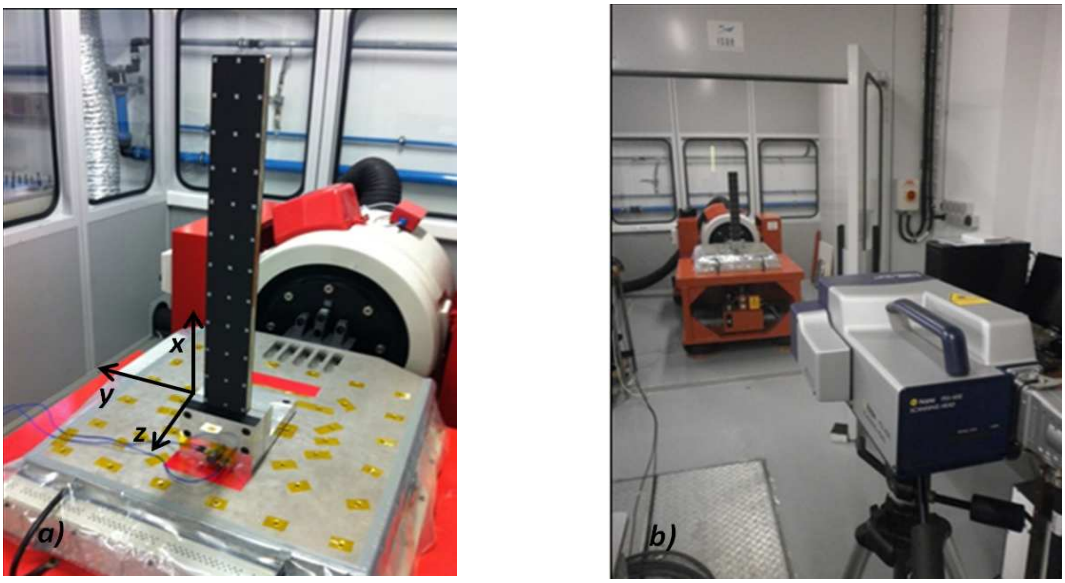

a) Beam embedded on the shaker. *b) Scanning Vibrometer.*

Figure 9 : Dynamic Experimental setup

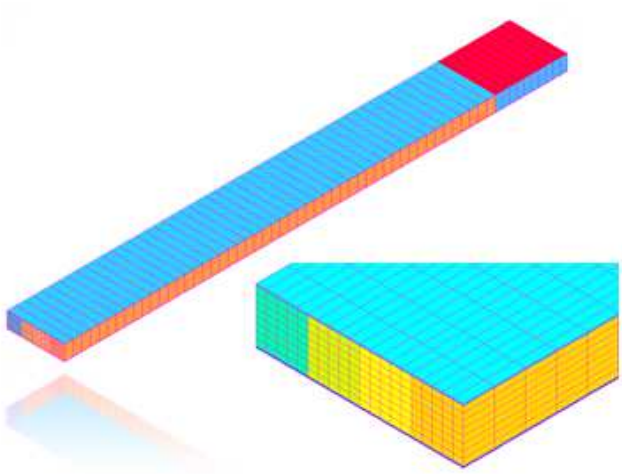

Figure 10 : Overview of the sandwich beam finite element model

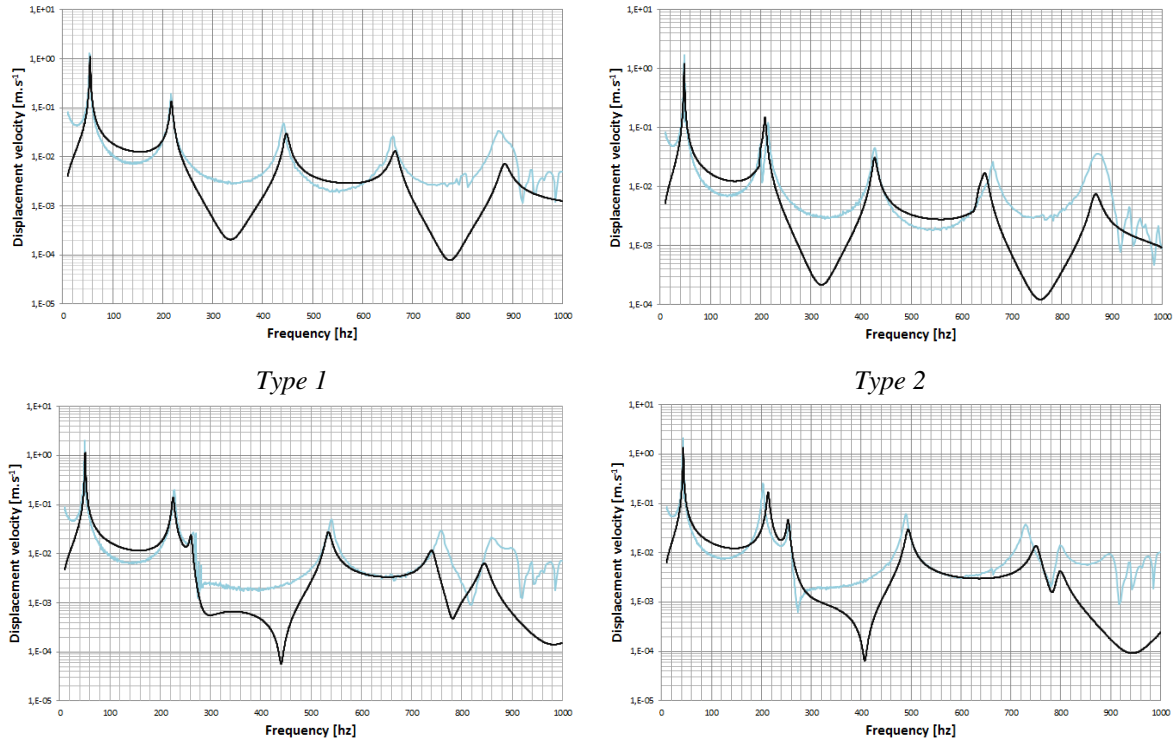

Type 1 *Type 2*

Type 3 *Type 4*

Figure 11: FRF comparison between simulation (black curve) and experiment (Blue curve)

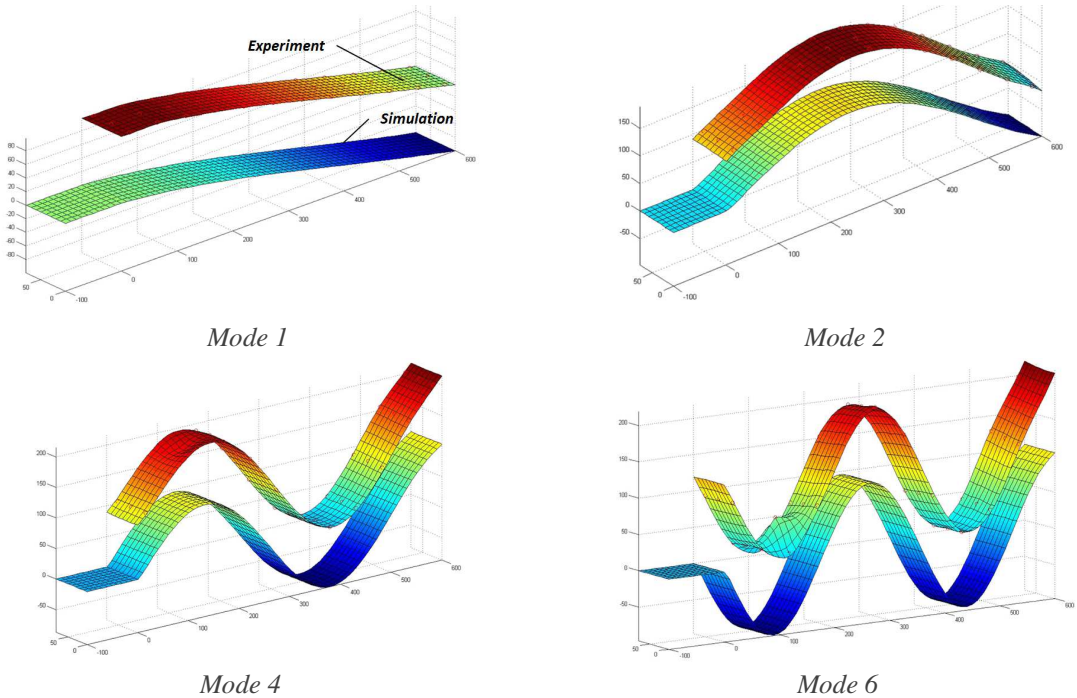

Mode 1 *Mode 2*

Mode 4 *Mode 6*

Figure 12 : Mode shapes of Type 1 beam configuration (Reference)

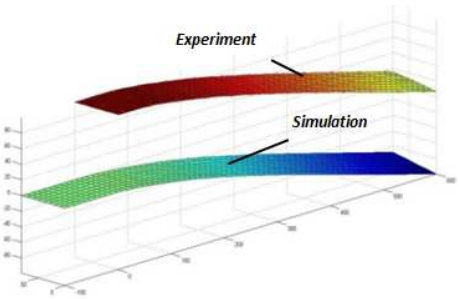

Mode 1

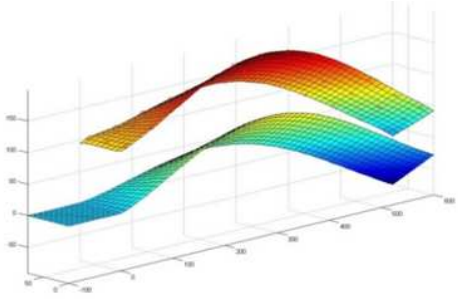

Mode 2

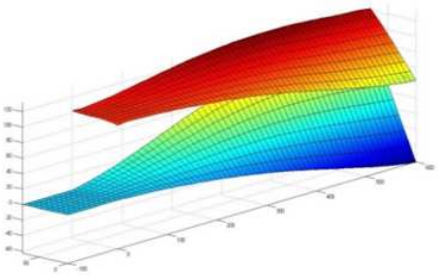

Mode 3

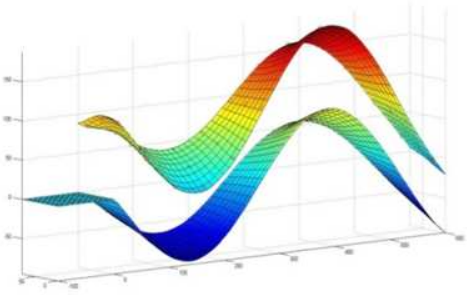

Mode 4

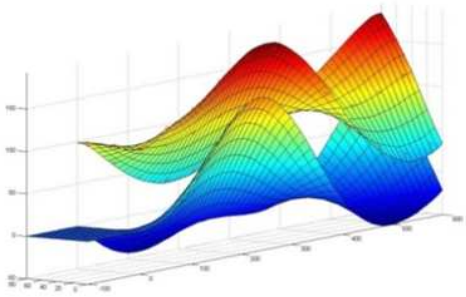

Mode 5

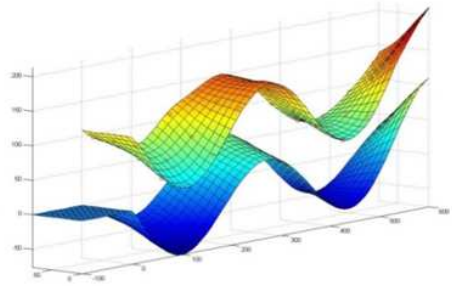

Mode 6

Figure 13 : Mode shapes of the Type 4 beam configuration (Fully coupled)

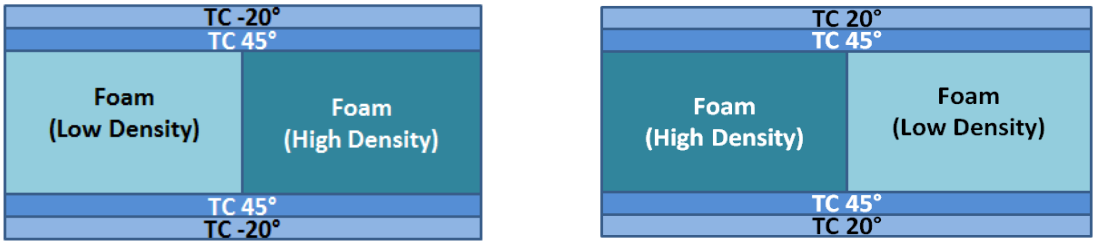

Type 5
Skin : External carbon ply at -20°/+70°
Core : Graded foam core

Type 6
Skin : External carbon ply at +20°/-70°
Core : Inverse Graded foam core

Figure 14 : Type 5 and Type 6 sandwich beam composition.

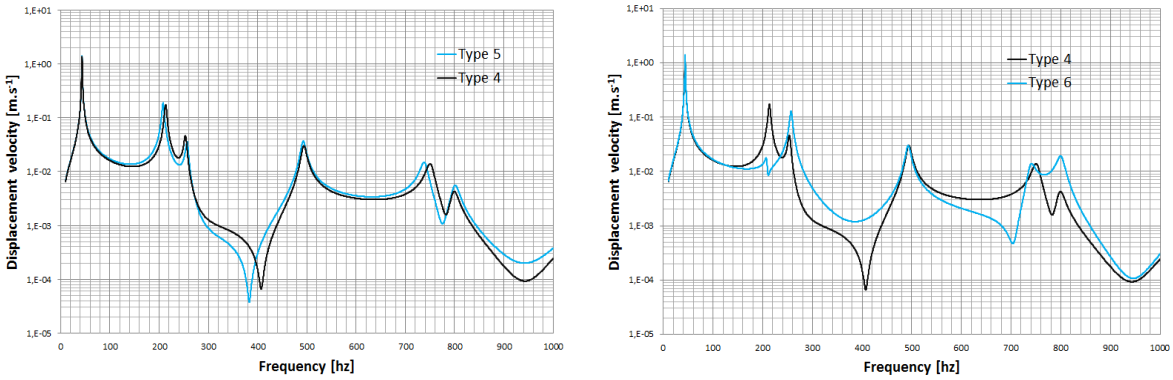

Figure 15: FRF curves of Type 4 (black curves), Type 5(blue curve left) and Type 6 (blue curve right) beam configurations

TABLES:

Section	Beam twist rate [°/m]	GJ [Mpa]	K_{45} [%GJ]	K_{43} [%GJ]
Box	0.430	6.35E+08	22.39%	0.03%
Elliptic	0.497	2.90E+08	24.10%	0.15%
Sandwich	1.318	6.06E+07	39.98%	1.99%

Table 1 : Inertia and structural bending-torsion coupling

Section	Beam twist rate [°/m]	Off axis ply [%]	Horizontally graded core [%]
Box	0.439	100%	0%
Elliptic	0.497	95%	5%
Sandwich	1.318	35%	65%

Table 2 : Influence of both technologies on the beam twist rate

Modes	Type 1			Type 2			Type 3			Type 4		
	Simu. [Hz]	Exp. [Hz]	Gap	Simu. [Hz]	Exp. [Hz]	Gap	Simu. [Hz]	Exp. [Hz]	Gap	Simu. [Hz]	Exp. [Hz]	Gap
1	54.06	53.75	-1%	47.25	47.86	1%	50.68	50.06	-1%	43.23	43,3	0%
2	197.43	-	-	192.34	199.6	4%	219.64	223.83	2%	210.69	204.23	-3%
3	210.46	210.94	0%	201.49	213.8	6%	255.07	260.77	2%	249.95	256.81	3%
4	429.72	433.12	1%	411.28	438.39	7%	520;30	530.53	2%	487.66	491.03	1%
5	616.70	-	-	609.65	662.06	9%	718.01	736.67	3%	737.30	725.6	-2%
6	636.61	645.00	1%	620.82	-	-	819.06	845.34	3%	786.46	801.34	2%

Table 3: Natural frequencies of the 6 first modes for all configuration types

		Orientated ply (Type 2)					
		1	2	3	4	5	6
Reference Sandwich beam (Type 1)	B1	99%	0%	0%	0%	0%	0%
	T1	0%	56%	46%	0%	0%	0%
	B2	0%	44%	53%	0%	0%	0%
	B3	0%	0%	0%	99%	0%	0%
	T2	0%	0%	0%	0%	91%	10%
	B4	0%	0%	0%	0%	9%	90%

Table 4: Identification matrix of the Type 2 configuration

Reference Sandwich beam (Type 1)		Graded foam core (Type 3)					
		1	2	3	4	5	6
	B1	99%	2%	1%	0%	0%	0%
	T1	0%	64%	37%	0%	0%	0%
	B2	0%	33%	61%	0%	2%	0%
	B3	0%	0%	0%	99%	0%	0%
	T2	0%	0%	0%	0%	95%	4%
	B4	0%	0%	0%	1%	3%	96%

Table 5: Identification matrix of the Type 3 configuration

Reference Sandwich beam (Type 1)		Inversed coupled sandwich beam (Type 4)					
		1	2	3	4	5	6
	B1	99%	1%	2%	0%	0%	0%
	T1	0%	14%	87%	0%	0%	0%
	B2	1%	84%	11%	0%	1%	0%
	B3	0%	1%	0%	98%	0%	1%
	T2	0%	1%	0%	0%	90%	10%
	B4	0%	0%	0%	1%	9%	88%

Table 6: Identification matrix of the Type 4 configuration

Reference Sandwich beam (Type 1)		Fully coupled sandwich beam (Type 5 & 6)					
		1	2	3	4	5	6
	B1	99%	2%	2%	0%	0%	0%
	T1	0%	38%	65%	0%	0%	0%
	B2	1%	58%	33%	1%	2%	1%
	B3	0%	1%	0%	95%	2%	0%
	T2	0%	0%	0%	2%	86%	11%
	B4	0%	0%	0%	1%	9%	87%

Table 7: Identification *matrix of the Type 5 and Type 6 configurations*